

Neuronal Excitability

Biophysical Basis of Alpha Rhythm Disruption in Alzheimer's Disease

Rohan Sharma and Suhita Nadkarni

<https://doi.org/10.1523/ENEURO.0293-19.2020>

Division of Biology, Indian Institute of Science Education and Research, Pune 411008, India

Abstract

Occipital alpha is a prominent rhythm (~10 Hz) detected in electroencephalography (EEG) during wakeful relaxation with closed eyes. The rhythm is generated by a subclass of thalamic pacemaker cells that burst at the alpha frequency, orchestrated by the interplay of hyperpolarization-activated cyclic nucleotide-gated channels (HCN) and calcium channels in response to elevated levels of ambient acetylcholine (ACh). These oscillations are known to have a lower peak frequency and coherence in the early stages of Alzheimer's disease (AD). Interestingly, calcium signaling, HCN channel expression and ACh signaling, crucial for orchestrating the alpha rhythm, are also known to be aberrational in AD. In a biophysically detailed network model of the thalamic circuit, we investigate the changes in molecular signaling and the causal relationships between them that lead to a disrupted thalamic alpha in AD. Our simulations show that lowered HCN expression leads to a slower thalamic alpha, which can be rescued by increasing ACh levels, a common therapeutic target of AD drugs. However, this rescue is possible only over a limited range of reduced HCN expression. The model predicts that lowered HCN expression can modify the network activity in the thalamic circuit leading to increased GABA release in the thalamus and disrupt the calcium homeostasis. The changes in calcium signaling make the network more susceptible to noise, causing a loss in rhythmic activity. Based on our results, we propose that reduced frequency and coherence of the occipital alpha rhythm seen in AD may result from downregulated HCN expression, rather than modified cholinergic signaling.

Key words: alpha rhythm; Alzheimer's disease; HCN; thalamic network

Significance Statement

Aggregation of amyloid- β , modified expression of ion channels and alterations in calcium signaling are hallmarks of Alzheimer's disease (AD) neurons. Separately, changes in the alpha rhythm is often an early observation in AD patients. We use a realistic computational model of the thalamus to elucidate the causal links between molecular changes in AD and their effect on alpha rhythm. Our model demonstrates that pathology of hyperpolarization-activated cyclic nucleotide-gated channels (HCN), crucial for alpha generation, alters calcium signaling, modifies excitation-inhibition balance in the thalamus makes the network more sensitive to noise. Our model, when seen in conjunction with diverse experimental data, posits a causal relationship between the formation of amyloid- β plaques, the downregulation of HCN channels and aberrations in the occipital alpha rhythm.

Introduction

Brain rhythms play a vital role in coordinating and organizing neuronal computations across various anatomic regions of the brain. These rhythms range from a fraction

of a hertz (delta) to over a hundred hertz (high gamma) and have been implicated in attention, spatial navigation, and memory consolidation (Buzsaki, 2006).

The authors declare no competing financial interests.

Author contributions: S.N. designed research; R.S. performed research; S.N. and R.S. contributed to analytic tools; R.S. analyzed data; R.S. and S.N. wrote the paper.

Received July 24, 2019; accepted February 2, 2020; First published March 11, 2020.

The alpha rhythm (7.5–12.5 Hz) in particular is associated with attention and semantic orientation (Rihs et al., 2007) and is seen to be modulated by changes in behavior (Buzsaki, 2006). In attention and discrimination tasks, the coherence in the alpha band measured from somatosensory and motor cortices decreases along with a concomitant increase in the power surrounding the 20-Hz band (Haegens et al., 2011). This indicates that coherence and frequency changes are functionally relevant attributes of the alpha rhythm. Apart from somatosensory and motor cortices, alpha band oscillations have also been observed in other brain regions like the prefrontal cortex (Halgren et al., 2002), auditory cortex (Tiihonen et al., 1991), and over the occipital lobe (Hughes and Crunelli, 2005). Alpha Rhythm activity over the occipital lobe, observed during relaxed, closed eye wakefulness (Berger, 1929; Hughes and Crunelli, 2005), is the focus of the present study.

Positron emission tomography (PET) and electroencephalography (EEG) recordings in humans indicate that the occipital alpha emerges from the interplay between cortical and thalamic neuronal networks (Schreckenberger et al., 2004). Upon muscarinic cholinergic activation, the *in vitro* local field potential (LFP) from the thalamus exhibits alpha band activity (Lőrincz et al., 2008). Additionally, application of muscarinic cholinergic antagonists to the thalamus [specifically to the lateral geniculate nucleus (LGN)] reduce alpha band frequency and power over the occipital region, as seen in EEG recordings of cats (Lőrincz et al., 2009). These alpha band oscillations over the occipital region, observed in EEG, are highly synchronized with the alpha band oscillations in the thalamic LFP (Hughes et al., 2011). Together, these studies indicate (1) a causal link between thalamic alpha oscillations and the alpha rhythm activity seen in EEG recordings over the occipital lobe and (2) cholinergic modulation as a trigger of thalamic alpha. While the alpha rhythm is a complex and ubiquitous phenomenon, observed over different anatomic areas during diverse behavioral states and arising from complex interactions between thalamocortical circuits, we restrict our investigation to the alpha rhythm originating in the thalamus during closed-eye relaxation and measured in EEG over the occipital region.

Patients of Parkinson's disease, Alzheimer's disease (AD), and other forms of dementia show distinct changes in their EEG recordings (Friston et al., 2015). In particular, lowering of the average dominant occipital alpha (DOA)

frequency in EEG recordings is seen across a population of AD patients (Vitiello, 1989; Crunelli et al., 2015; Blinowska et al., 2017). As mentioned before, the frequency and power of both the thalamic alpha rhythm (observed in the LFP) and the occipital alpha rhythm (recorded in EEG) are modulated by the concentration of ambient acetylcholine (ACh; Lőrincz et al., 2008, 2009; Hughes et al., 2011). A class of drugs that inhibit the breakdown of ACh (acetylcholinesterase inhibitors), and therefore augment its resting levels, can provide temporary symptomatic relief in AD. They are also shown to increase occipital alpha rhythm frequency and coherence (Babiloni et al., 2013). These observations, along with recent studies which show that thalamic degeneration precedes symptoms of cognitive decline in AD (De Jong et al., 2008; Aggleton et al., 2016), suggest a link between AD, the thalamic alpha rhythm and cholinergic signaling.

We investigate different biochemical changes associated with AD using a realistic computational model of the thalamic network (Vijayan and Kopell, 2012) that generates the alpha rhythm. The network consists of thalamocortical cells (TCs), reticular cells (REs) and specialized TC cells, the so-called HTC cells due to the expression of certain high-threshold calcium channels (more details in methods). Individual HTC cells generate intrinsic oscillations due to the interplay between the high threshold calcium current and hyperpolarization-activated cyclic nucleotide-gated channels (HCN) channels. Consistent with the extant literature (Hughes et al., 2011), thalamic alpha in our model arises from this intrinsic activity of HTC neurons which synchronize via gap-junctions. These cells fire at ~10 Hz when the ambient level of ACh is high enough to activate muscarinic ACh receptors (mAChRs; Lőrincz et al., 2008). Amyloid- β plaques are a characterizing feature of AD. Separately, lowered HCN channel expression in brain slices of AD patients was shown to cause an increase in the production of amyloid- β peptide (Saito et al., 2012). Apart from changes in cholinergic signaling, these observations provide an additional correspondence between the alpha rhythm and AD, mediated by HCN channels and calcium signaling. Our study examines the causal links between the biochemical changes observed in AD and quantifies the changes in the thalamic network dynamics that underlie a modified thalamic alpha rhythm.

Materials and Methods

The thalamic network

The alpha rhythm originates in HTC cells that innervate and receive input from the rest of the thalamic network. The HTC neurons are synchronized to each other via gap-junctional connectivity. Our model is a scaled down motif of the thalamic network (Fig. 1) and based on the model proposed by Vijayan and Kopell (2012). The model is the canonical model (Destexhe and Sejnowski, 1997) of the thalamocortical circuitry, with the addition of a high-threshold T-type calcium current in 20% of the TC cells (HTC; Fig. 1). It consists of two HTC cells coupled via

This work was supported by the Wellcome Trust/DBT India Alliance Grant IA/I/12/1/500529; the Department of Science and Technology (DST), Government of India awarded to S.N.; the Innovation in Science Pursuit for Inspired Research (INSPIRE); the DST/INSPIRE Fellowship 2016/IF60611; and the Indian Institute of Science Education and Research Pune.

Correspondence should be addressed to Suhita Nadkarni at suhita@iiserpune.ac.in.

<https://doi.org/10.1523/ENEURO.0293-19.2020>

Copyright © 2020 Sharma et al.

This is an open-access article distributed under the terms of the Creative Commons Attribution 4.0 International license, which permits unrestricted use, distribution and reproduction in any medium provided that the original work is properly attributed.

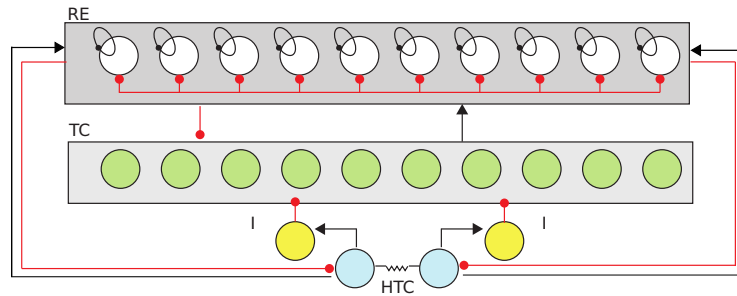


Figure 1. Thalamic network involved in alpha generation. The network described here consists of the reticular cells (REs), the thalamocortical neurons (TC cells) and high-threshold TCs (HTC). The RE cells (white) mutually inhibit each other and inhibit all of the TC cells (green). TC cells send excitatory connections to all of the RE cells. There are no direct mutual connections between TC cells. The HTC cells (blue), responsible for generating the α rhythm, inhibit the TC cells via sending an excitatory drive to the inhibitory-interneurons (yellow). The ratio of the RE to TC cells is 1:1 and 20% of the TC cells are HTC cells. The inhibitory interneurons are modeled implicitly as an inhibitory synapse from HTCs to TCs with a time delay. Gap-junctions between the HTC cells enable synchronized bursting.

gap-junctions that provide an excitatory drive to RE cells and an inhibitory drive to TC cells. The TC cells are excitatory and connect to all RE cells but not to each other or HTC cells. The RE cells are GABAergic and inhibit every other cell in the network including other RE cells (Fig. 1). The HTC cells receive a white-noise input with zero mean which was implemented using the Euler-Maruyama method. The TC and RE neurons receive a Poisson-distributed train of excitatory and inhibitory impulses. The activation of the mAChRs is modeled by lowering the potassium leak conductance (McCormick and Prince, 1986; Vijayan and Kopell, 2012).

Code accessibility

Simulations were performed on a high-performance computing cluster (HP PROLIANT SL230s Gen8 as compute nodes, each with two CPUs containing 10 cores each; CPU: Intel(R) Xeon(R) CPU EV-2860 v2 2.80 GHz) with 1464 processing units housed in IISER Pune. We used an in-house Computational Neuroscience library written in C++ to perform the simulations. The code described in this paper is freely available at <https://github.com/rhnsrma/ENEURO0293-19.2020>. The time step of each simulation was taken to be 0.01 ms.

Quantitative details of HTC cells

Our investigation primarily concerns HTC cells as they are the locus of all manipulations. The details of TC cells, RE cells and synapses are presented later.

$$C \frac{dV_{HTC}}{dt} = -I_{Na} - I_K - I_{TLT} - I_{THT} - I_L - I_H - I_{AHP} - I_{GJ} - I_{GABA_A} - I_{GABA_B} + I_{APP}. \tag{1}$$

Potassium current:

$$I_K = g_K n^4 (V - E_K) \quad \text{here:} \quad \frac{dn}{dt} = \frac{n_\infty(V) - n}{\tau_n(V)},$$

$$n_\infty(V) = \frac{\alpha_n(V)}{\alpha_n(V) + \beta_n(V)} \quad \tau_n(V) = \frac{1}{\alpha_n(V) + \beta_n(V)},$$

where:

$$\alpha_n = \frac{0.032(15 - V_t)}{\exp((15 - V_t)/5.0) - 1}$$

$$\beta_n = 0.5 \exp((10 - V_t)/40).$$

$$V_t = V_{HTC} + 25, \quad g_K = 10 \text{mS/cm}^2 \quad \text{and} \quad E_K = -100 \text{mV}.$$

Sodium current:

The m_∞ ; τ_m ; h_∞ ; and; τ_h have equations identical to the n_∞ and the τ_n of the potassium gate n.

$$I_{Na} = g_{Na} m^3 h (V - E_{Na}), \quad \frac{dm}{dt} = \frac{m_\infty(V) - m}{\tau_m(V)},$$

$$\frac{dh}{dt} = \frac{h_\infty(V) - h}{\tau_h(V)},$$

where:

$$\alpha_{m_m} = \frac{0.32(13 - V_t)}{\exp((13 - V_t)/4.0) - 1}$$

$$\beta_m = \frac{0.28(V_t - 40)}{\exp((V_t - 40)/5) - 1}$$

$$\alpha_{h_h} = 0.128 \exp((17 - V_t)/18)$$

$$\beta_h = \frac{4}{\exp((40 - V_t)/5) + 1}$$

$$V_t = V_{HTC} + 25, \quad g_{Na} = 90 \text{mS/cm}^2 \quad \text{and} \quad E_{Na} = +50 \text{mV}.$$

Low-threshold calcium current:

$$I_{TLT} = g_{TLT}m^2h(V - E_{Ca}), \quad m = m_{\infty}(V),$$

$$\frac{dh}{dt} = \frac{h_{\infty}(V) - h}{\tau_h(V)},$$

where:

$$m_{\infty}(V) = \frac{1}{\exp(-(57 + V_t)/6.2) + 1}$$

$$h_{\infty} = \frac{1}{1 + \exp((V_t + 81.0)/4.0)},$$

$$\tau_h = \frac{30.8 + \left(\frac{211.4 + \exp(V_t + 113.2)/5.0}{1 + \exp(V_t + 84.0)/3.2} \right)}{3.74}$$

$$\frac{d[Ca]}{dt} = \frac{-10I_{TLT}}{2 \times 96489} + \frac{0.00024 - [Ca]}{5.0}$$

If the first term is negative, it is set to zero. $g_{TLT} = 2mS/cm^2$, $V_t = V_{HTC} + 2$ and the reversal potential for calcium is calculated using the Nernst equation.

High-threshold calcium current:

$$I_{THT} = g_{THT}m^2h(V - E_{Ca}), \quad m = m_{\infty}(V),$$

$$\frac{dh}{dt} = \frac{h_{\infty}(V) - h}{\tau_h(V)},$$

where:

$$m_{\infty}(V) = \frac{1}{\exp(-(40.1 + V)/3.5) + 1}$$

$$h_{\infty} = \frac{1}{1 + \exp((V_t + 62.2)/5.5)},$$

$$\tau_h = 0.1483\exp(-0.09398 * V) + 5.284\exp(0.008855 * V).$$

$$\frac{d[Ca]}{dt} = \frac{-10(I_{TLT} + I_{THT})}{2 \times 96489} + \frac{0.00024 - [Ca]}{3.0}$$

The first term must be positive, otherwise it is set to zero.

In the model described by Vijayan and Kopell (2012), the calcium concentrations in HTC neurons experienced by the two calcium channels, I_{THT} and I_{TLT} , are different. We do not make this additional assumption. In our model, both I_{THT} and I_{TLT} channels, sense the same intracellular calcium. We adjust for this change by using values of g_{THT} and g_{Kleak} which produce stable 10-Hz oscillations in HTC cells.

$g_{THT} = 12mS/cm^2$ (modified from Vijayan and Kopell, 2012)

E_{Ca} is calculated using the Nernst equation.

Leak current:

$$I_L = g_L(V - E_L) + g_{KL}(V - E_{KL}),$$

where:

$$g_L = 0.01mS/cm^2, E_L = -70mV, g_{KL} = 0.01mS/cm^2,$$

$$E_{KL} = -100mV.$$

The effect of ACh is modeled as a lowered potassium leak conductance g_{Kleak} (the details will be discussed in Results; see Eq. 5; Vijayan and Kopell, 2012; Krishnan et al., 2016).

H-current:

$$I_H = g_h r(V - E_h), \quad \frac{dr}{dt} = \frac{r(V) - r_{\infty}}{\tau_r(V)},$$

where:

$$r_{\infty} = \frac{1}{1 + \exp((V + 60)/5.5)},$$

$$\tau_r = 20 + \frac{1000}{\exp((V + 56.5)/14.2) + \exp(-(V + 74)/11.6)}$$

$$g_h = 0.36mS/cm^2, \text{ and } E_h = -40mV.$$

Calcium-activated potassium current:

$$I_{AHP} = g_{AHP}m^2(V - E_K), \quad \frac{dm}{dt} = \frac{m_{\infty} - m}{\tau_m},$$

where:

$$m_{\infty} = \frac{48[Ca]^2}{48[Ca]^2 + 0.09}$$

$$\tau_m = \frac{1}{48[Ca]^2 + 0.09}$$

$$g_{AHP} = 15mS/cm^2, \text{ and } E_K = -100mV.$$

Gap-junction current:

$$I_{GJ} = g_{GJ}(V_{HTC} - V_{post}),$$

where V_{post} is the membrane potential of the neuron that is connected to this HTC neuron by a gap-junction

$$g_{GJ} = 0.003 - 0.005 mS/cm^2.$$

In reality, the HTC cells receive inputs from various other neurons. Under the diffusion limit of synaptic noise, where the weights are very small and there are a lot of Poissonian synaptic inputs, the synaptic noise can be modeled as Gaussian white noise (Lánská et al., 1994). The HTC cells are also subject to thermal noise, channel conductance fluctuations and channel shot noise (Gerstein and Mandelbrot, 1964). These fluctuations occur at timescales that are much faster than any timescales in the biophysical model. These sources of noise can be modeled cumulatively as a low amplitude Gaussian white-noise. The HTC cells receive a Gaussian distributed white noise through the stochastic Euler-Maruyama integrator (this noise is not present in results shown in Fig. 2):

$$\frac{dV_{HTC}}{dt} = -\sum I_{channels} + \sqrt{dt} \times \xi(t) \quad (2)$$

where $\xi(t)$ is drawn from a Gaussian distribution with mean 0 and variance 0.1.

Entropy measure

V_i is the membrane voltage of the HTC neurons, where $i \in \{1,2\}$

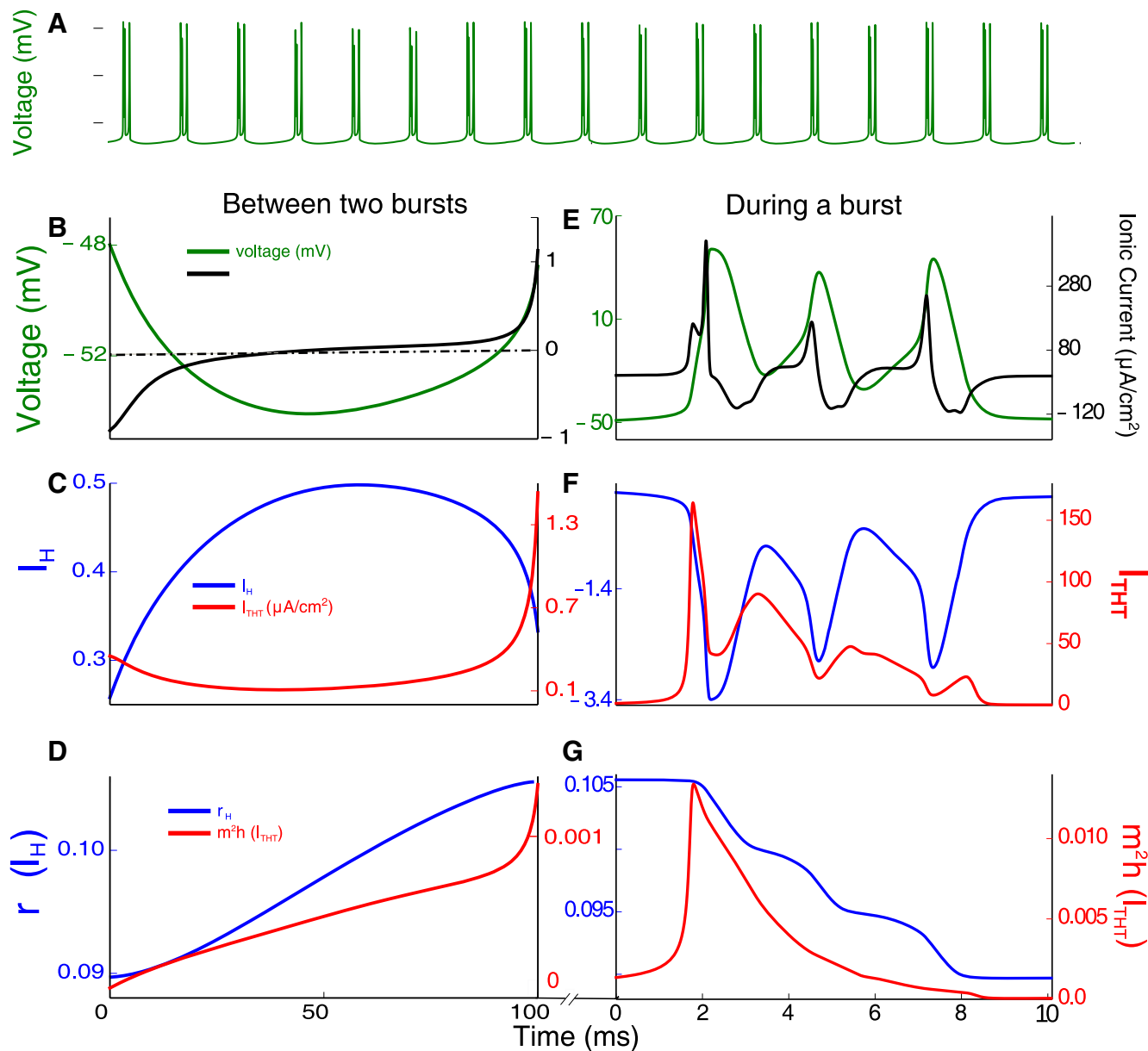


Figure 2. Chronology of events underlying the thalamic alpha. **A**, The interburst interval determines the 10-Hz rhythm underlying the thalamic alpha. Membrane voltage (green) of a single HTC neuron as it goes through bursts of activity. **C**, **D**, Activity of relevant ion channels between the bursts for the duration of a 100-ms time window. **F**, **G**, Activity of the same channels during the 10-ms burst of the cell. **B**, Slowly increasing membrane voltage (green) due to the increase in I_H conductance (blue, **B**) during repolarization of the membrane potential by the potassium current. The total current (black) increases with I_H . The bursting activity is initiated by activation of I_{THT} current (red, **E**, **F**) and terminated by repolarization due to the potassium current. **C**, The hyperpolarization-activated current I_H (blue) increases slowly during membrane repolarization leading to eventual activation of the I_{THT} (red). **D**, Gating variables of the I_H (r_H , blue) and I_{THT} (m^2h , red) currents. The high-threshold calcium current gets activated around the ~ 90 -ms mark. **E**, The increase in I_{THT} activates the fast sodium channels and triggers a series of APs. Membrane potential (green) and total ionic current in the immediate 10 ms after the activation of I_{THT} . This burst of APs is initiated by I_H and I_{THT} in that order (left panel). **F**, The high-threshold calcium current (red) provides a depolarizing impetus that sustains a burst of APs. The I_H (blue) current becomes hyperpolarizing above -40 -mV membrane voltage but does not contribute much in this phase due to low conductance values compared with the high-threshold calcium. **G**, The slow decay of the gating variables of the I_H (blue) as the membrane potential rises above the activation voltage. The gating variables of I_{THT} (red) slowly deactivate at high voltages during APs.

$$LFP(t) = \frac{(V_1(t) + V_2(t))}{2}.$$

Before performing the discrete fast Fourier transformation (DFFT), the LFP trace is smoothed by taking a simple moving average over a window of 10 ms (which corresponds to 25 discrete points as our observation frequency in 2.5 kHz; Eq. 3), and the mean is subtracted from each data point to make the new mean zero. We smoothed the LFP trace to suppress contributions to the power spectrum from high-frequency noise. The moving average with 10-ms time window will damp contributions to the power spectrum from frequencies above 60 Hz. This is sufficient for our purposes as we are interested in frequencies around the 4- to 30-Hz range. The filtering makes the entropy of the Fourier transform a cleaner measure of aperiodicity.

$$LFP'(t_i) = \frac{\sum_{j=i-24}^i LFP(t_j)}{25} - \frac{\sum_{j=1}^N LFP(t_j)}{N} \quad (3)$$

$$F(\omega) = DFFT(LFP'(t))$$

$$p(\omega) = \frac{|F(\omega)|^2}{\int_0^\infty |F(\omega)|^2 d\omega}$$

$p(\omega)$ is the probability distribution function which is used to calculate the Shannon entropy:

$$entropy = -\sum_{\omega_i} p(\omega_i) \log(p(\omega_i)). \quad (4)$$

Quantitative details of TC cells and RE cells
Thalamo-reticular (RE) neurons

$$C \frac{dV_{RE}}{dt} = -I_{Na} - I_K - I_{TRE} - I_L - I_{GABA_A} - I_{AMPA} + I_{EPSP} + I_{IPSP}. \quad (6)$$

Potassium current:

$$I_K = g_K n^4 (V - E_K) \quad \frac{dn}{dt} = \frac{n_\infty(V) - n}{\tau_n(V)},$$

here:

$$n_\infty(V) = \frac{\alpha_n(V)}{\alpha_n(V) + \beta_n(V)} \quad \tau_n(V) = \frac{1}{\alpha_n(V) + \beta_n(V)},$$

where:

$$\alpha_n = \frac{0.032(15 - V_t)}{\exp((15 - V_t)/5.0) - 1}$$

$$\beta_n = 0.5 \exp((10 - V_t)/40)$$

$$V_t = V_{RE} + 55, \quad g_K = 10 \text{ mS/cm}^2 \quad \text{and} \quad E_K = -100 \text{ mV}.$$

Sodium current:

The m_∞ ; τ_m ; h_∞ ; and τ_h have equations identical to the n_∞ and the τ_n of the potassium gate n.

$$I_{Na} = g_{Na} m^3 h (V - E_{Na}), \quad \frac{dm}{dt} = \frac{m_\infty(V) - m}{\tau_m(V)},$$

$$\frac{dh}{dt} = \frac{h_\infty(V) - h}{\tau_h(V)},$$

where:

$$\alpha_m = \frac{0.32(13 - V_t)}{\exp((13 - V_t)/4.0) - 1}$$

$$\beta_m = \frac{0.28(V_t - 40)}{\exp((V_t - 40)/5) - 1}$$

$$\alpha_h = 0.128 \exp((17 - V_t)/18)$$

$$\beta_h = \frac{4}{\exp((40 - V_t)/5) + 1}$$

$$V_t = V_{RE} + 55, \quad g_{Na} = 100 \text{ mS/cm}^2 \quad \text{and} \quad E_{Na} = +50 \text{ mV}.$$

Calcium current:

$$I_{TRE} = g_{TRE} m^2 h (V - E_{Ca}), \quad \frac{dm}{dt} = \frac{m_\infty(V) - m}{\tau_m(V)},$$

$$\frac{dh}{dt} = \frac{h_\infty(V) - h}{\tau_h(V)},$$

where:

$$m_\infty(V) = \frac{1}{\exp(-(52 + V)/7.4) + 1},$$

$$\tau_m = 0.99 + \frac{0.333}{\exp((V + 27)/10) + \exp(-(V + 102)/15)}$$

$$h_\infty = \frac{1}{1 + \exp((V + 80.0)/5.0)},$$

$$\tau_h = 28.307 + \frac{0.33}{\exp((V + 48)/4) + \exp(-(V + 407)/50)}.$$

$$\frac{d[Ca]}{dt} = \frac{-10I_{TRE}}{2 \times 96489} + \frac{0.00024 - [Ca]}{3.0}$$

The first term must be positive, otherwise it is set to zero. $g_{TRE} = 2.3 \text{ mS/cm}^2$ and the reversal potential for calcium is calculated using the Nernst equation.

Leak current:

$$I_L = g_L (V - E_L) + g_{KL} (V - E_{KL}),$$

where:

$$g_L = 0.01 \text{ mS/cm}^2, \quad \text{and} \quad E_L = -73 \text{ mV}$$

$$g_{KL} = 0.08 \text{ mS/cm}^2, \quad \text{and} \quad E_{KL} = -100 \text{ mV}.$$

Poisson noise (I_{IPSP} and I_{EPSP}):

The applied current is a train of Poisson-distributed excitatory and inhibitory impulses. The details of the same will be discussed in the following section.

Thalamo-cortical (TC) neurons

$$C \frac{dV_{TC}}{dt} = -I_{Na} - I_K - I_{TLT} - I_L - I_H - I_{GABA_A} - I_{GABA_B} + I_{EPSP}. \quad (7)$$

Potassium current:

The potassium current follows the same dynamics as the potassium current in HTC cells.

Sodium current:

The sodium current follows the same dynamics as the sodium current in HTC cells.

Low-threshold calcium current:

The low threshold calcium current follows the same dynamics as the low threshold calcium current in HTC cells.

Leak current:

$$I_L = g_L(V - E_L) + g_{KL}(V - E_{KL}),$$

where:

$$g_L = 0.01\text{mS/cm}^2, E_L = -70\text{mV}, g_{KL} = 0.0028\text{mS/cm}^2, \\ E_{KL} = -100\text{mV}.$$

H-current:

$$I_H = g_h(o + a \times (1 - c - o))(V - E_h),$$

$$\frac{do}{dt} = 0.0001(1.0 - c - o) - 0.001((1.0 - p)/0.01),$$

$$\frac{dp}{dt} = 0.0004(1.0 - p) - 0.004\left(\frac{[Ca]}{0.0002}\right)^2,$$

$$\frac{dc}{dt} = \beta_c o - \alpha_c c$$

where:

$$\alpha_c = \frac{h_\infty}{\tau_s}, \quad \beta_c = \frac{1 - h_\infty}{\tau_s},$$

$$h_\infty = \frac{1}{1 + \exp((V + 75)/5.5)},$$

$$\tau_s = 20 + \frac{1000}{\exp((V + 71.5)/14.2) + \exp(-(V + 89)/11.6)}$$

$$g_L = 0.1\text{mS/cm}^2, a = 2 \text{ and } E_h = -43\text{mV}.$$

Poisson noise (I_{EPSP}):

The applied current is a train of Poisson-distributed excitatory and inhibitory impulses. The details are given below.

Firing rate:

The firing rate shown in Figure 7 (presented later) was obtained by counting the number of times the voltage of the cell crossed 0 mV during the simulation and then dividing that number by the duration of the simulation (~14 s). The firing rates for all the TC and RE neurons were then averaged for all the cells and all the 5 trials.

Noise:

$$I_{EPSP} = -g_s \exp(T(t) - t)(V - 0) \\ I_{IPSP} = -g_s \exp(T(t) - t)(V + 85)$$

where:

$$T(t) = \min\{T_1, T_2, \dots, T_{n-1}, T_n, \dots, |t < T(t)\}.$$

The difference between the impulse times, T_1, T_2, \dots, T_n is an exponentially distributed random variable with a mean of 10 ms for TC and RE cells.

For RE cells:

$g_s = 0.02\text{mS/cm}^2$ for EPSPs and $g_s = 0.015\text{mS/cm}^2$ for IPSPs.

TC neurons are stimulated with EPSPs with but no IPSPs:

$$g_s = 1.0\text{mS/cm}^2.$$

Quantitative details for synapses

AMPA:

$$I_{AMPA} = g_{AMPA}[R](V - E_{AMPA})$$

$$\frac{d[R]}{dt} = 0.98[T](1 - [R]) - 0.180[R].$$

[T] is the transmitter concentration. In response an action potential (AP) the transmitter concentration is increased to 0.5 mM and stays there for 0.3 ms for HTC and 0.5 ms for TC cells. [R] represents the fraction of the receptors that are open.

$$E_{AMPA} = 0\text{mV}$$

$$g_{AMPA} : \text{HTC} \Rightarrow RE = 0.001, \text{TC} \Rightarrow RE = 0.05$$

GABA_A:

$$I_{GABA_A} = g_{GABA_A}[R](V - E_{GABA_A})$$

$$\frac{d[R]}{dt} = 20[T](1 - [R]) - 0.180[R].$$

[T] is the neurotransmitter concentration. In response an AP the transmitter concentration is increased to 0.5 mM and stays there for 1.0 ms for HTC and 0.3 ms for RE cells. [R] represents the fraction of the receptors that are open.

$$E_{GABA_A} = -85\text{mV},$$

$$g_{GABA_A} : \text{HTC} \Rightarrow \text{TC} = 0.4(\text{with a delay of } 10\text{ms})$$

$$RE \Rightarrow \text{HTC} = 0.0002, RE \Rightarrow \text{TC} = 0.002, RE \Rightarrow$$

$$RE = 0.02$$

GABA_B:

$$I_{GABA_B} = g_{GABA_B} \left(\frac{[G]^4}{[G]^4 + 100} \right) (V - E_{GABA_B})$$

$$\frac{d[G]}{dt} = 0.18[R] - 0.034[G]$$

$$\frac{d[R]}{dt} = 0.09[T](1 - [R]) - 0.0012[R]$$

[T] is the neurotransmitter concentration. In response an AP the transmitter concentration is increased to 0.5 mM and stays there for 0.3 ms. [R] represents the fraction of the receptors that are open. [G] is the concentration of the G protein that gets activated on agonization of the receptors.

$$E_{GABA_B} = -95\text{mV}$$

$$g_{GABA_B} : RE \Rightarrow \text{HTC} = 0.004\text{mS/cm}^2,$$

$$RE \Rightarrow \text{TC} = 0.004\text{mS/cm}^2.$$

Results

Ionic current dynamics that determine the thalamic alpha timescale

We first describe the activity of a single HTC cell (no noise) to elucidate the mechanisms that generate the characteristic 10-Hz timescale of the alpha rhythm. The chronology of events that result in the generation of the rhythm in the presence of ACh is described in Figure 2. High-threshold calcium ion channels and a non-specific (for ions) HCN channel are the ionic components of HTC cells that govern the rhythm. The precision and robustness of this rhythm are determined by the intrinsic dynamics of the gating variables of each current and the interplay between the currents mediated by membrane voltage and calcium. After each burst of APs, the cell undergoes a brief hyperpolarization that activates the HCN channels (I_H ; Fig. 2B, blue). This leads to a slow positive inward current (Fig. 2B) that steadily depolarizes the cell until it reaches the threshold voltage where calcium channels, I_{THT} , open (Fig. 2B, red). These calcium channels are activated near instantaneously above the threshold but inactivated over a much slower timescale (Fig. 2E, F, red). Further, these channels open only within a narrow voltage range (approximately -50 to -10 mV). The calcium current causes a rapid depolarization (Fig. 2B), triggering the fast sodium channel leading to a burst of APs (Fig. 2E). The slow inactivation gate of the calcium channel leads to the slow decay of the calcium current that eventually terminates the burst of APs (Fig. 2E–G). This allows the potassium channel to repolarize the membrane. As the membrane repolarizes, the HCN channels get activated, setting the system up for another cycle (for a summary of these events, please see Fig. 3). The timescale of depolarization determines the interval between bursts and thus the frequency of the alpha rhythm. The depolarization timescale is determined by the magnitude of the I_H current, which, in turn, depends on the conductance and expression of HCN channels.

Effect of varying HCN expression in HTC cells on the thalamic alpha

In the temporal lobe of patients with sporadic AD, reduced expression of HCN channels has been reported (Saito et al., 2012). Further, suppressed HCN expression is also shown to accelerate amyloid- β aggregation in cell cultures (Neuro2a, a fast-growing mouse neuroblastoma cell line; Saito et al., 2012). Prompted by these observations, we investigate the precise effect of lowered HCN expression seen in AD on the occipital alpha rhythm. We varied the conductance of the I_H current (g_H) to mimic the effect of changes in HCN expression in HTC cells (Fig. 4A). The control value for the conductance, set to 0.36 mS/cm² (Vijayan and Kopell, 2012), generates 10-Hz rhythm. We quantified the periodicity of the rhythm using the power spectral entropy of the LFP (for details, see Materials and Methods). Higher values of entropy imply that the power in the signal is distributed over various frequencies. A periodic time series will exhibit low entropy,

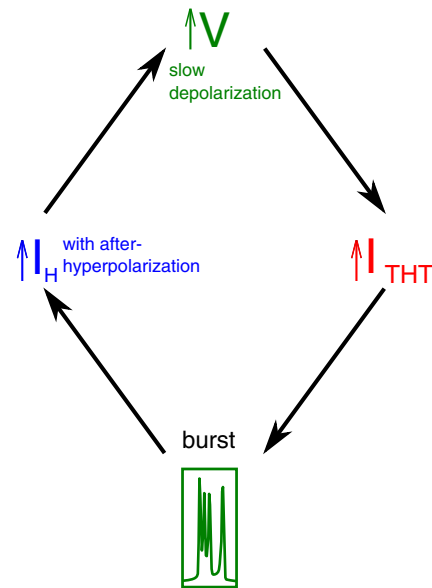


Figure 3. Schematic illustrating the chronology of events. After a burst, the cell membrane hyperpolarizes to subthreshold voltages. This activates the I_H current which slowly depolarizes the membrane voltage. This leads to the activation of the I_{THT} current, which in turn, triggers another burst.

as the power would be confined to only a few narrow frequency regions (Fig. 5C).

Reducing g_H over a limited range from 120% to 70% of the control value (0.36 mS/cm²), monotonically reduced the frequency of HTC firing (Vijayan and Kopell, 2012). Reduction in g_H has the effect of reducing the interburst interval of HTC cells (Fig. 2C). Peak frequency from power spectra is shown in Figure 4A, blue open circles. For $g_H < 0.27$ mS/cm² and > 0.43 mS/cm² (Fig. 4A at the boundary of the shaded region), periodicity breaks down and alpha rhythm is lost. This is seen as an increase in entropy (Fig. 4A, orange filled diamonds). Increased expression of I_H channels (higher value of g_H) makes the membrane more excitable, because of which small fluctuations are more likely to cross the firing threshold, resulting in the noisy firing. Decreased expression of HCN, on the other hand, delays the onset of I_{THT} (Fig. 2). At values of g_H below 0.27 mS/cm², the HTC cell membrane remains near the firing threshold over long periods of time. This makes the system sensitive to background noise which is now more likely to generate a supra-threshold perturbation leading to a spike. Our results show that the alpha rhythm is highly sensitive to HCN expression, as periodic activity of HTC cells is possible only over a limited regime of HCN expression.

Limited rescue of the thalamic alpha with ACh

Increase in ambient ACh increases the excitability of HTC cells and initiates alpha. We hypothesize that, in early AD, reduced HCN expression in HTCs leads to lower excitability and delays the activation of the burst inducing calcium current. The chain of events that determine the timescale of the rhythm now take longer to complete. To

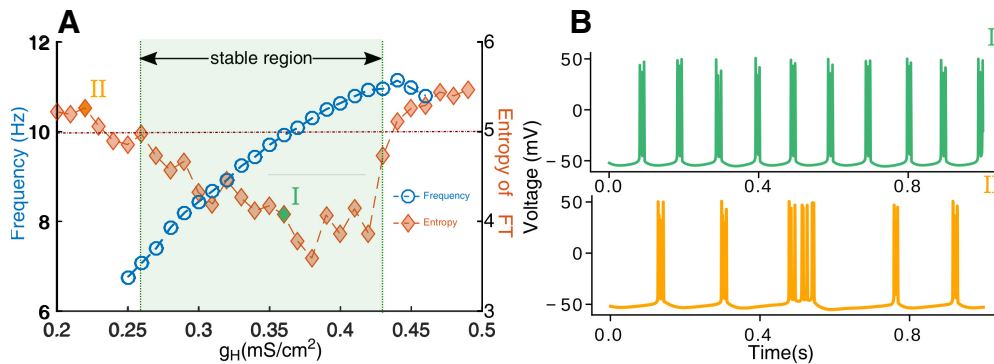


Figure 4. Monotonic dependence of the peak frequency by varying HCN expression. **A**, The intrinsic oscillation frequency (blue, open circles) of HTC cells shows a monotonic dependence over a limited range of HCN expression (g_H ; marked as the stable region). However, beyond this range continued HCN overexpression (right of the stable region) leads to HTC cells losing periodicity (due to overexcitability). In the other direction (left of the stable region), low levels of HCN expression makes the system more sensitive to noise, resulting in a loss of periodicity again. There exists an optimal regime of g_H where bursting is regular. This is depicted as lower entropy (orange, filled diamonds) for a range of g_H . **B**, Illustrative voltage traces of HTC cells from the stable region, particularly $g_H = 0.36$ mS/cm² and unstable region ($g_H = 0.22$ mS/cm²).

understand the extent to which increased ACh levels can counter the effect of lowered HCN expression and recover the alpha rhythm. In Figure 5, different levels of HCN expression (green: normal; black: reduced to ~80% of control) are shown and their effect on the alpha rhythm are described. We define η_{ach} as a measure of the fractional change in cholinergic activity.

$$\eta_{ach} = \frac{g_{Kleak_norm} - g_{Kleak_mod}}{g_{Kleak_norm}} \times 100 \quad (\%). \quad (5)$$

Where g_{Kleak_norm} is the potassium leak conductance value that results in a 10-Hz alpha rhythm and g_{Kleak_mod} is the modified potassium leak. Increase in ambient ACh levels (η_{ach}) leads to a monotonic increase in the alpha frequency. Power spectra for healthy, pathologic and rescue cases of the alpha rhythm are shown in Figure 5C-I-III. Increasing η_{ach} by ~20% from its normal value was able to rescue the alpha rhythm (Fig. 5C/III) in cells with reduced HCN expression (black, ~80% of control). However, the increased excitability of HTC cells due to an increase in η_{ach} also makes them more susceptible to noise. The loss of periodicity was quantified as an increase in power spectral entropy (filled diamonds). Here, we clearly see that rescue by ACh is possible only within a limited range of reduced HCN levels. For HCN levels as low as 45% of control (Fig. 5B) we observed that increases in ACh cannot bring the HTC rhythm up to 10 Hz and periodicity is restricted to frequencies below 9 Hz (Fig. 5C/IV).

We explore a wide range of cholinergic tone (changing the potassium leak conductance) and HCN expression (g_H) to find the range over which the network shows periodic oscillations. Periodic oscillations in the HTC cells are observed only over a limited regime of HCN expression (g_H) and cholinergic tone (η ; Fig. 6) marked by lower entropy (blue).

Lowering g_H can lead to an enhanced GABA activity

Several studies have characterized modified occipital alpha in AD (Vitiello, 2015). Thus far we have shown how

changes in ACh levels and HCN channel expression in the thalamus can modulate thalamic alpha (as the underlying basis for changes in occipital alpha). Next, we analyzed the effect of changing the alpha frequency, as seen in AD, on the dynamics of the thalamic network in our model. The decrease in the frequency of alpha was implemented as a decrease in I_H conductance (g_H ; Fig. 4A). This predictably leads to a lower frequency of HTC firing. Under these pathologic conditions of decreased HTC activity, the TC cells that were suppressed via GABAergic drive from the rhythm generating HTCs (Fig. 1) were released from inhibition. A corresponding increase in TC activity is seen in Figure 7A. The increase in TC activity causes the RE cells to fire at higher rates (Fig. 7B). The RE cells also receive excitation from HTC cells. The increase in RE firing rate happens despite the decreased drive from HTCs to the REs. This is because the HTC cells account for only 20% of the total excitatory drive to REs. The larger number of TCs (four times the number of HTCs) creates a positive feedback loop, causing an increase in RE activity. The enhanced activity of RE cells, in turn, enhances the inhibitory feedback to HTC cells reducing their frequency further (Fig. 7). The overall effect is thus an increase in GABAergic activity. While the increased presence of the neurotransmitter GABA has been reported in the astrocytes in the dentate gyrus (DG) of AD mice (Wu et al., 2014), we predict that lowered HCN expression can also tilt the balance between excitation and inhibition in the thalamic network. Our model suggests that lowered alpha rhythm frequency in the thalamus can cause a cascade of changes in thalamic network activity and may ultimately result in increased inhibition of HTC cells.

Calcium current and its interaction with HCN expression in HTC cells

Elevated levels of cytosolic calcium linked to dysregulation in the calcium signaling are a common observation in AD neurons (Berridge, 2014). In order to simulate the pathology, we investigated the effect of changes in

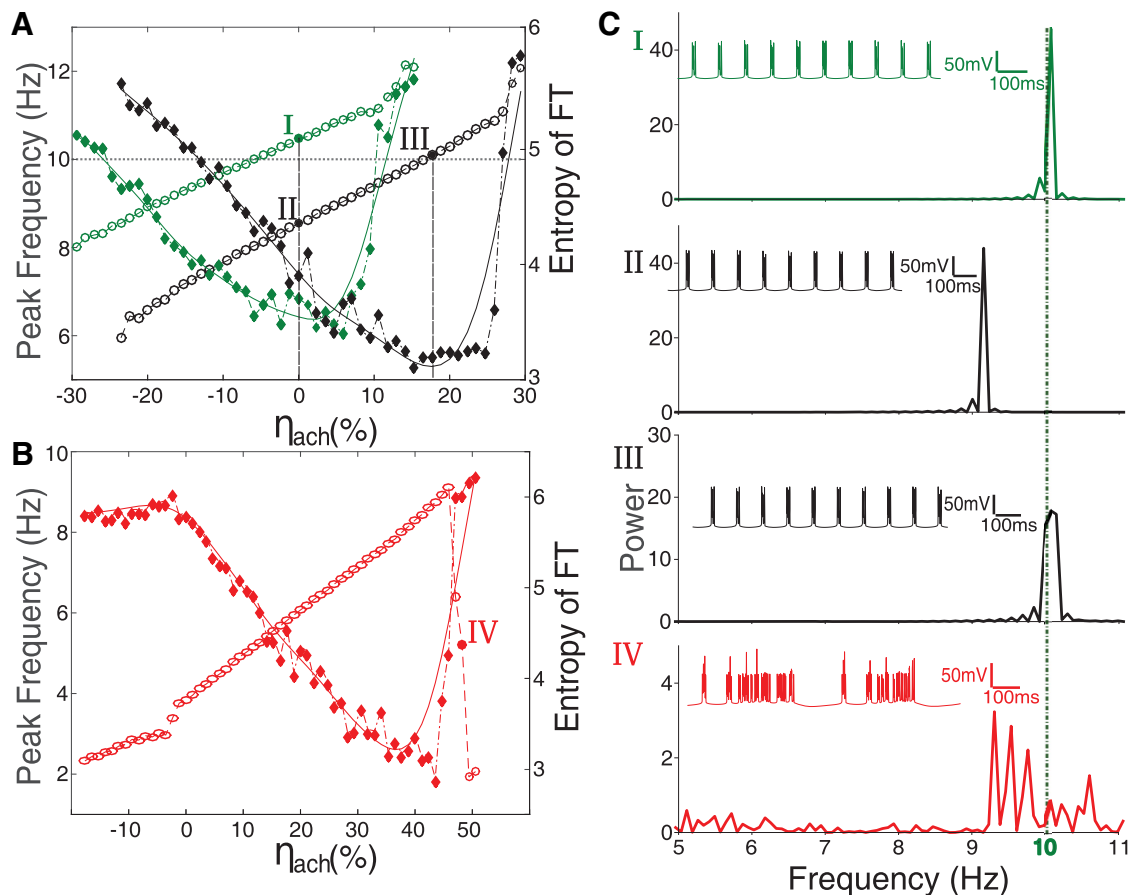


Figure 5. Rescue of the thalamic alpha with changing levels of basal [ACh] and HCN channel expression. **A**, Increasing ambient ACh levels (η_{ach}) increases the peak frequency of the rhythm (open circles, green for control HCN expression and open circles, black for I_H expression reduced to 80% of control). Peak frequencies remain lower than control when HCN expression is compromised to mimic known observations in AD (compare voltage traces shown in the insets of I and II in **C**). The lowered frequency of alpha as a result of lower g_H can be rescued by increasing ACh levels. For example, 20% reduction in g_H (80% of control) needs $\sim 18\%$ increase in ACh (see voltage trace in the inset of III in **C**). There appears to be a threshold of ambient ACh levels beyond which entropy (filled diamonds; green for normal and black for reduced HCN expression) increases dramatically, suggesting a loss in periodicity. The overall entropy also remains high for decreased g_H . **B**, Severe reduction in HCN expression (45%, red) results in a lowered frequency of alpha and cannot be rescued by increasing ACh levels. With 45% g_H expression, HTC cells can achieve a maximum rhythm of 9 Hz before a complete breakdown of regular firing. This is seen as a sudden rise in entropy (filled red diamonds). **C**, Power spectra corresponding to I, II, and III from **A** and IV from **B**. Insets show the time series of the LFP corresponding to the Fourier transform.

conductance of the high-threshold calcium current (g_{THT}) that is crucial for the alpha rhythm, for a range of HCN expressions (g_H ; Fig. 8A; MacManus et al., 2000). The control system for each of the HCN expressions were initially set-up to generate 10-Hz frequency by appropriately changing the potassium leak conductance (see legend in Fig. 8A). Increased cytosolic calcium (pathologic state) corresponds to enhanced calcium entry via high-threshold calcium channels (corresponding to positive changes in g_{THT} in Fig. 8A). Interestingly, varying the conductance of the high-threshold calcium current does not change the frequency of the alpha rhythm significantly in our model. However, they can cause the HTC cells to lose coherence (Fig. 8A). As calcium conductance is changed, HTC cells go through regimes of periodic and irregular firing. These changes in periodicity can be seen in the sudden transitions in spectral entropy in Figure 8A. The burst of APs in HTC cells arises from the depolarizing current,

of the high-threshold calcium channels (Fig. 2). After each AP, there is a competition between the amplitude of the hyperpolarizing potassium current and depolarizing calcium current, which determines whether the cell goes through another AP. The inactivation timescale of the calcium current dictates the number of APs in a burst. Increasing the conductance of the calcium current increases the duration over which APs can be generated. This is because it takes longer for the high threshold calcium current to decay to a value such that the potassium current can terminate the burst. This also implies that the amplitude of calcium current at the end of a burst for each “instantiation” of calcium conductance, will correspond to a different value of the potassium current. Thus, the number of APs in a burst increases with increasing conductance of the high-threshold calcium current. The regimes of chaotic activity illustrated in Figure 8A corresponds to the intermediate values of calcium conductance, as we

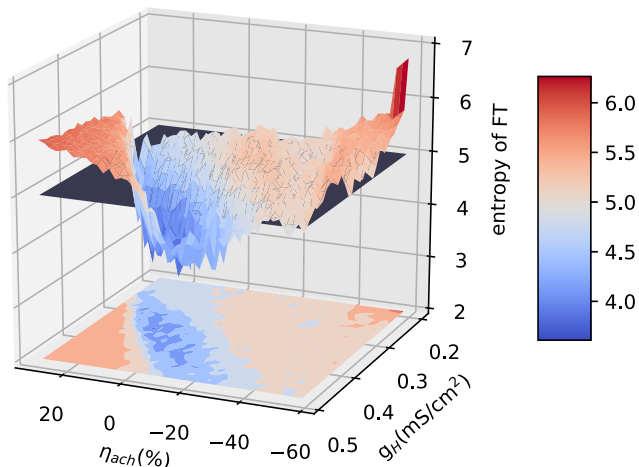


Figure 6. Parameter analysis for stable oscillations for a range of HCN expression and ACh levels. Higher entropy (red) implies aperiodicity in oscillations. The system transitions to aperiodicity at approximately entropy = 5.0 (demarcated by the black plane in the figure). There is a limited range of ACh and HCN expression over which stable oscillations are seen.

go from n number of APs in a burst to $n + 1$ APs (range of n is 2–4). In these intermediate values of calcium conductance, the magnitudes of potassium and calcium currents are balanced at the end of the burst and background noise can randomly push the HTC cell toward another AP or hyperpolarize it to subthreshold voltages. This leads to periods of irregular firing for intermediate values of calcium conductance and non-monotonic dependence of periodicity on calcium current.

The range of calcium conductance over which regular alpha activity is maintained decreases with decreasing g_H (compare dark red with black in Fig. 8A). Healthy cells ($g_H = 0.36$ mS/cm²; Fig. 8A, black) appear robust and can tolerate as much as a 25% increase in the calcium conductance before losing periodicity. On the other hand, decreasing g_H values, to simulate the pathologic condition of lowered HCN expression shows lower tolerance for changes in calcium conductance. Figure 8A also describes the response to increased HCN expression (light green and dark green). The tolerance to increase in calcium is seen to systematically decrease with decrease in g_H (Fig. 8B). The heightened sensitivity to calcium is also seen as narrower troughs in the entropy (windows of regular firing) for the pathologic condition of lower expression of HCN (dark red and red traces in Fig. 8A). Lowering HCN expression (g_H) corresponds to a systematic reduction in the tolerance to changes in calcium (summarized in Fig. 8B).

Discussion

AD is a catastrophic disease that implicates multiple brain areas resulting in a range of symptoms. While precise molecular mechanisms that underlie the constellation of deficits and the causal links between them are not completely clear, several, apparently independent hypotheses have been proposed to delineate the root

pathology. The most prominent of these relate to the toxic effects of accumulating amyloid- β plaques and Tau fibrils, a characteristic feature of AD (Binder et al., 2005). While amyloid- β and Tau-fibrils disrupt a wide array of signaling pathways in the brain, we do not yet have a complete understanding of the biochemistry that leads to their accumulation and proliferation. The calcium hypothesis of Alzheimer's suggests that dysfunctional regulation of the calcium signaling profoundly vitiates neural functions like memory formation and consolidation by modifying synaptic plasticity and other signaling cascades. However, it is not known how minor changes in the calcium signaling cause drastic changes in behavior (Berridge, 2014). The cholinergic hypothesis proposes a reduced release of ACh as an early cause of the symptoms associated with AD (Drachman and Leavitt, 1974). In support of this, the most prevalent drugs administered to AD patients that provide temporary symptomatic relief are acetylcholinesterase inhibitors (Selkoe, 1997; Kumar et al., 2015) that increase the life span of ambient ACh. EEG studies report a reduction in power and frequency of the occipital alpha in a majority of AD patients as compared with control subjects (Vitiello, 1989; Hughes and Crunelli, 2005; Blinowska et al., 2017). Given the crucial role played by ACh signal in orchestrating occipital alpha (Lórinicz et al., 2009; Krishnan et al., 2016), these observations suggest compromised cholinergic signaling underlying its modification in AD.

Analysis of causal relationships between HCN expression, alpha rhythm, and amyloid- β aggregation

Cognitive decline, including poor navigational ability, is observed before amyloid- β plaques are detected in AD (Allison et al., 2016). HCN expression in the entorhinal cortex regulates grid-cell formation and is essential for navigation (Giocomo et al., 2011). Interestingly it is also seen that drugs like Sildenafil, that enhance HCN activation, temporarily bring cognitive relief without affecting the amyloid- β load (Cuadrado-Tejedor et al., 2011). This suggests that compromised regulation in HCN expression can be one of the possible early changes triggering AD symptoms. HCN channels play a multitude of roles in the brain (Narayanan and Johnston, 2008; Honnuraiah and Narayanan, 2013) and aberrant expression of these channels have been associated with many pathologies (Herrmann et al., 2007; Blumenfeld, 2016). For a more comprehensive review of the role of HCN channels in neurodegenerative diseases see Chang et al. (2019). Observation of reduced HCN expression being correlated with over-expression of amyloid- β in AD neurons (Saito et al., 2012) is of particular interest to the present investigation.

We explore the space of all possible causal relationships between amyloid- β ($A\beta$), HCN channel expression (g_H) and modified thalamic alpha rhythm in AD. We have established that lowering the HCN channel expression, shown to be correlated with the occipital alpha rhythm, reduces the thalamic alpha rhythm frequency and coherence (Fig. 4; Hughes et al., 2011). The first box in Figure 9A lists all the possibilities, where I_H current channels (g_H) do not disrupt the alpha rhythm. Given the insights from

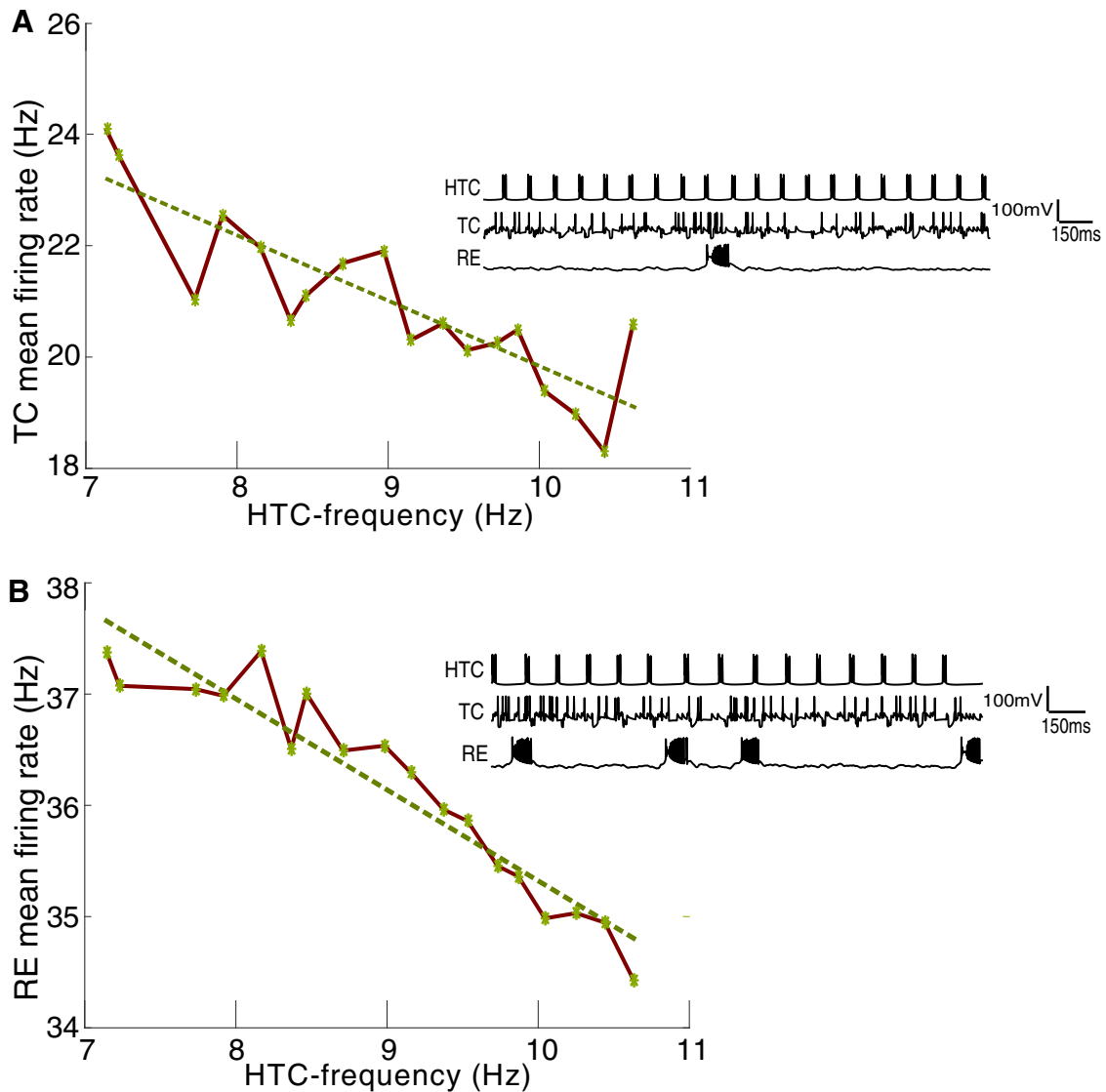


Figure 7. Increase in inhibitory activity follows a reduction in the firing rate of HTC cells. **A**, There is an inverse relationship between HTC and TC firing. Lower drive from HTCs releases the inhibitory drive (via interneurons) on the TC cells causing an increase in their activity. Inset shows the time series of HTC, TC, and RE activity corresponding to a normal rhythm (10-Hz HTC frequency, $g_H = 0.36$ mS/cm²). **B**, Inverse relationship between HTC firing and RE firing. Increased activity of the TC cells leads to enhanced RE activity. Inset shows the time series of HTC, TC, and RE activity corresponding to lowered HTC activity of 7.5 Hz due to reduced HCN expression ($g_H = 0.28$ mS/cm²).

our model (a monotonic relationship between HCN expression and alpha peak frequency and coherence seen in Fig. 4), we can exclude these relationships. Postmortem studies of brains AD subjects have lower levels of HCN channels when compared with non-AD subjects (Saito et al., 2012). In studies where the HCN channels were knocked out (KO), Saito et al., report increased amyloid- β aggregation when compared with wild-type (WT) neurons (Saito et al., 2012). They also show that using an HCN channel blocker (ZD7288) in WT leads to similar levels of amyloid- β accumulation as the KO neurons. Statistically, these results suggest a relationship between reduced HCN expression and amyloid- β . Saito et al. (2012) also showed that HCN forms a complex with the amyloid-precursor protein (APP) *in vivo* and *in*

vitro, suggesting a possible mechanism for HCN regulation of amyloid- β production. Using these observations, the relationships described in the second box which represents all other relationships in which HCN does not affect amyloid- β load can be eliminated (Fig. 9B). Our model combined with experimental observations reduces the list of relationships to merely three that are illustrated in the third box in Figure 9C. HCN channel expression affects both the alpha rhythm and amyloid- β directly. However, it is not yet clear if there is a directed link connecting amyloid- β and the alpha rhythm.

In light of the role of HCN expression in AD and the insights from the model, we propose that aberrant HCN expression may be a causal link to modified occipital alpha

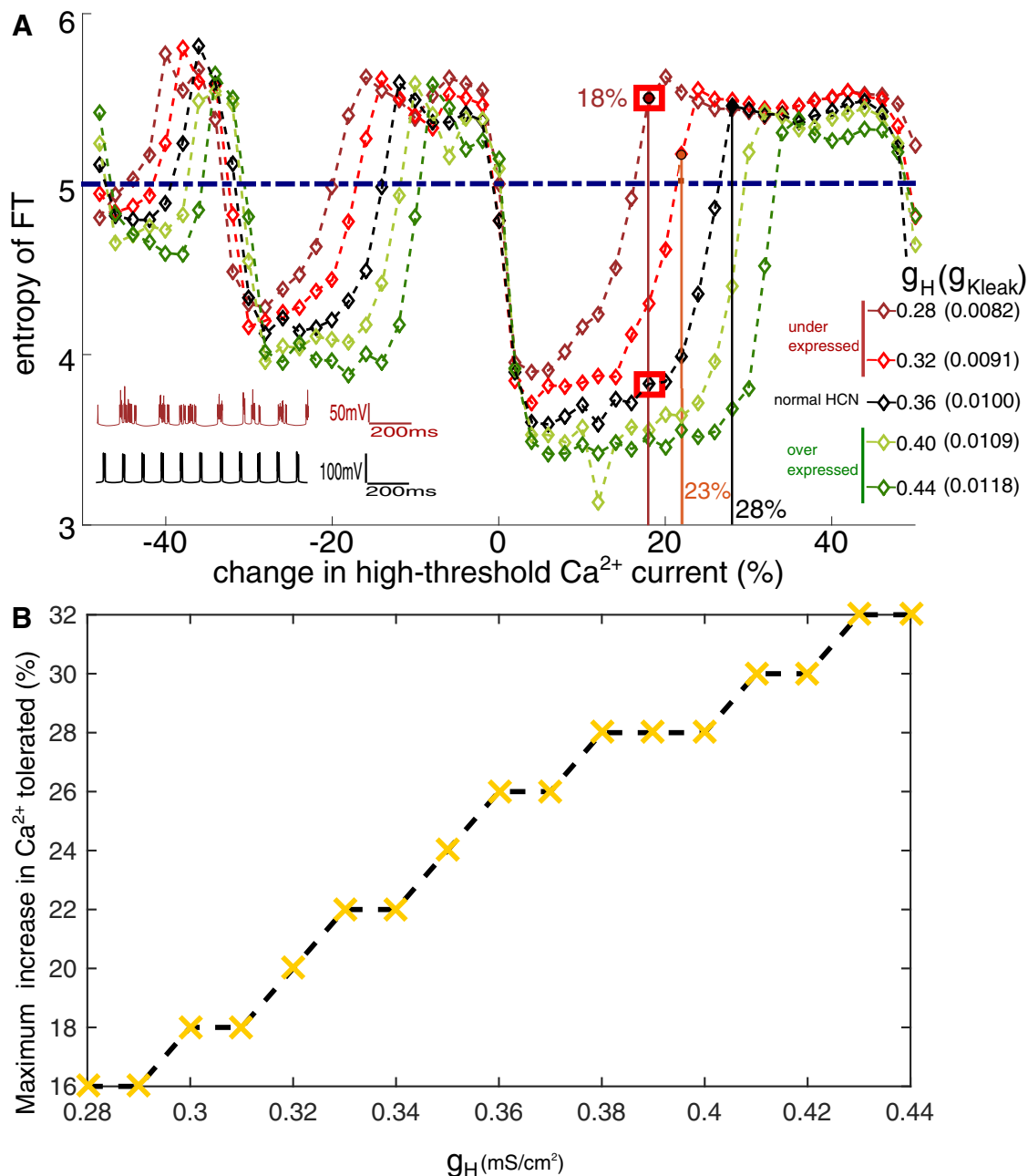


Figure 8. Lowered HCN makes the thalamic alpha more sensitive to small changes in the calcium conductance. **A**, Colored lines show deviations from normal HCN expression levels. Systematically varying the calcium conductance in both directions leads to sudden increases in the entropy describing incoherent firing of the HTC cells. Lower HCN expression ($g_H = 0.28$ and 0.32 mS/cm², maroon and red) have a lower tolerance for changes in calcium. This is seen as narrower windows of low entropy compared with the normal expression of HCN ($g_H = 0.36$ mS/cm² black). Inset shows time series of the LFP when calcium conductance is enhanced by ~18% for reduced HCN expression (maroon, $g_H = 0.28$ mS/cm², irregular firing) and normal HCN expression (black, $g_H = 0.36$ mS/cm², regular 10-Hz firing). Horizontal line (dashed dark blue) marks the threshold (5.0) for entropy beyond which we see irregular firing. **B**, Tolerance to changes in calcium conductance decreases with decrease in HCN expression. For calcium conductance above the threshold value associated with each g_H , irregular firing is seen.

in AD. Downregulated HCN activity and expression may precede and possibly trigger excessive amyloid- β aggregation. AD is a multifaceted disease and ultimately invokes several cascading changes in the cells and extracellular biochemistry. We propose that HCN under-expression is one of the crucial early pathologies by

which a regulatory breakdown can lead to excessive amyloid- β plaque build-up.

Mechanisms for loss in coherence

We characterize two distinct mechanisms that lead to a loss of coherence and lower power in alpha as observed

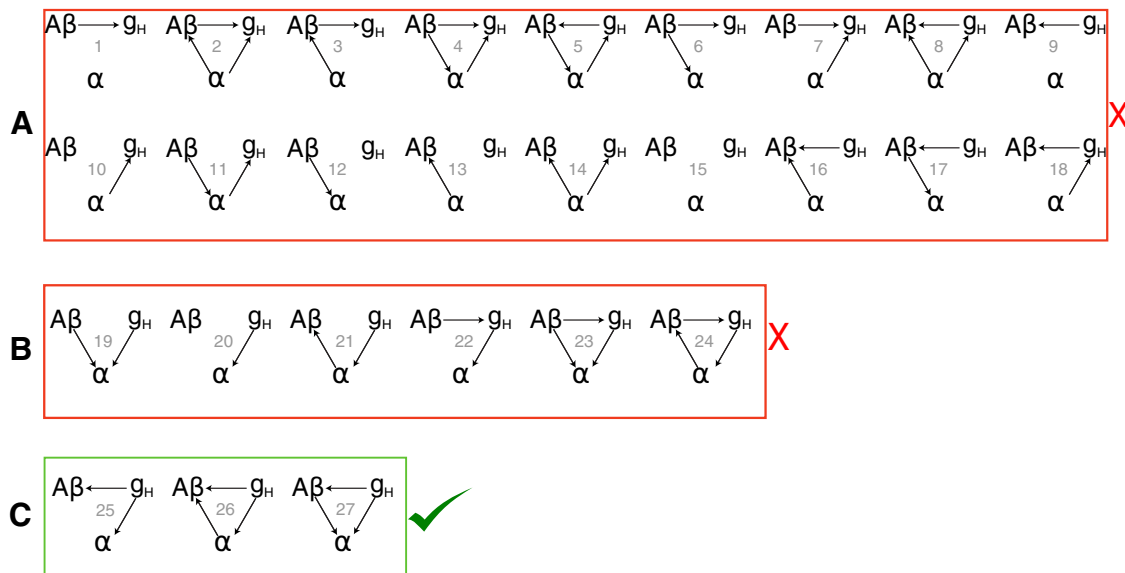


Figure 9. Potential causality between amyloid- β plaques ($A\beta$), HCN channels (g_H), and the α rhythm (α). **A**, HCN expression directly affects the thalamic α rhythm. Therefore, we can eliminate the possibilities where HCN expression does not affect the thalamic α rhythm. **B**, The appearance of β -amyloid plaques and lowered expression of HCN channels are strongly correlated and therefore not independent of each other, in fact, lowered HCN expression has been shown to cause increased amyloid- β aggregation (Saito et al., 2012). We can eliminate all relationships where HCN expression does not affect amyloid- β . **C**, Three possible causal relationships.

in AD. (1) A loss of coherence with increased ACh is due to increased cell excitability. We demonstrate how excessive cholinergic modulation in the thalamic network leads to a sudden loss of coherence (Fig. 5A, green, $\eta_{ach} > 15\%$). Under these circumstances, a random background signal has a lower barrier to cross the threshold for initiating a burst, hence the exact time of initiating the burst underlying the alpha rhythm becomes unreliable. The same mechanism also underlies the loss in coherence with increasing g_H (Fig. 4, $g_H > 0.43$ mS/cm²). (2) Under control conditions (Fig. 10A), the HCN expression lies within a region where the cell does not spend too much time near the burst threshold, and at the same time has a substantial barrier to cross to reach the threshold. This allows for a robust 10-Hz burst to be precisely orchestrated that is predominantly unaffected by noise. Figure 10B illustrates how Reducing HCN expression (lower g_H) reduces the rate at which the membrane depolarizes (Fig. 10B). The compensatory effect of increasing cholinergic tone can lower the threshold for initiating the burst to maintain the 10-Hz timescale of the rhythm (ΔT in the figure 10). However, this leads to an increased probability of noise initiating a burst imprecisely.

Alpha Rhythm relation to overall firing rates and extracellular GABA

A recent study on transgenic mouse models of AD implicates enhanced GABAergic drive (Wu et al., 2014). In these studies, a temporary rescue of cognitive function was observed by reducing the inhibitory effect of GABA. Our model illustrates that higher GABA levels can be a direct downstream effect of lower frequency of the thalamic alpha rhythm due to reduced HTC firing frequency (Fig. 7).

Reduction in HCN expression to mimic the AD pathology increases global firing rates. This is a consequence of the reduction in HTC firing frequency leading to a reduction in the inhibition on the TC cells. This, in turn, increases the activity in the GABA releasing RE cells (Fig. 7). Thus, a lower alpha will lead to increased activity of both TC and RE cells, this is consistent with the observation of normal alpha being associated with suppression of neuronal firing (Klimesch, 2012). In summary, our model predicts both an increase in overall activity and increased GABA levels in

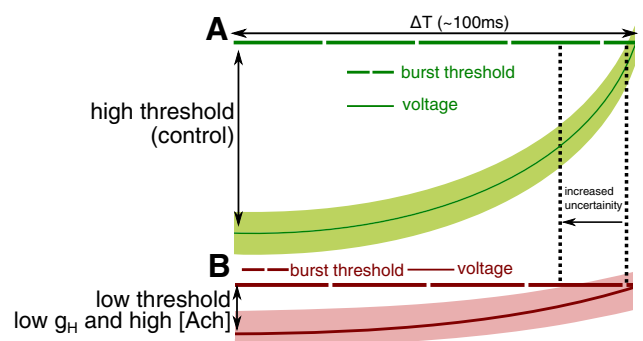


Figure 10. Illustration of the limited rescue of α rhythm. **A**, Control: I_H current steadily depolarizes the membrane voltage (dark-green solid line) until it reaches the threshold for a burst (dark-green broken line). The light-green band around the voltage trace signifies the uncertainty in the membrane voltage due to noise. **B**, Low g_H and high ACh: under these modified conditions the expected time taken for the voltage to reach the burst threshold is the same, but the noise, in this case, takes it closer to the burst threshold.

the thalamus under pathologic conditions of reduced alpha in AD.

Conclusion

Using an alpha rhythm generating network model of the thalamus, we have systematically elucidated the causal links between different molecular changes associated with AD and their effect on the thalamic alpha. We hypothesize that HCN pathology causes thalamic alpha rhythm disruption, precedes amyloid- β plaque formation and may underlie early cognitive deficiency in the disease. Our results illustrate the limitations of therapeutic interventions that involve enhancing ACh. We predict the downstream effects of changes in thalamic alpha, leading to enhanced GABA activity. Mimicking increased calcium flux as seen in AD, results in global changes in network firing rate and a loss of coherence in the occipital alpha rhythm. When the HCN pathology is simulated, network activity becomes highly sensitive to small changes in calcium signaling and background noise. Often, disrupted brain rhythms are an early change associated with AD, our model can contribute to our understanding of early pathogenesis of the disease.

References

- Aggleton JP, Pralus A, Nelson AJ, Hornberger M (2016) Thalamic pathology and memory loss in early Alzheimer's disease: moving the focus from the medial temporal lobe to papez circuit. *Brain* 139:1877–1890.
- Allison SL, Fagan AM, Morris JC, Head D (2016) Spatial navigation in preclinical Alzheimer's disease. *J Alzheimers Dis* 52:77–90.
- Babiloni C, Del Percio C, Bordet R, Bourriez JL, Bentivoglio M, Payoux P, Derambure P, Dix S, Infarinato F, Lizio R, Triggiani AI, Richardson JC, Rossini PM (2013) Effects of acetylcholinesterase inhibitors and memantine on resting-state electroencephalographic rhythms in Alzheimer's disease patients. *Clin Neurophysiol* 124:837–850.
- Berger H (1929) On the electroencephalogram of man. *Arch Psychiatrie* 87:527–570.
- Berridge MJ (2014) Calcium regulation of neural rhythms, memory and Alzheimer's disease. *J Physiol* 592:281–293.
- Binder LI, Guillozet-Bongaarts AL, Garcia-Sierra F, Berry RW (2005) Tau, tangles, and Alzheimer's disease. *Biochim Biophys Acta* 1739:216–223.
- Blinowska KJ, Rakowski F, Kaminski M, De Vico Fallani F, Del Percio C, Lizio R, Babiloni C (2017) Functional and effective brain connectivity for discrimination between Alzheimer's patients and healthy individuals: a study on resting state EEG rhythms. *Clin Neurophysiol* 128:667–680.
- Blumenfeld H (2016) Epilepsy and consciousness. In: *The neurology of consciousness* (Laureys S, Gosseries O, Tononi G, eds), Ed 2, Chapter 16, pp 255–270. San Diego: Academic Press.
- Buzsaki G (2006) *Rhythms of the brain*. New York: Oxford University Press.
- Chang X, Wang J, Jiang H, Shi L, Xie J (2019) Hyperpolarization-activated cyclic nucleotide-gated channels: an emerging role in neurodegenerative diseases. *Front Mol Neurosci* 12:141.
- Crunelli V, David F, Lőrincz ML, Hughes SW (2015) The thalamocortical network as a single slow wave-generating unit. *Curr Opin Neurobiol* 31:72–80.
- Cuadrado-Tejedor M, Hervias I, Ricobaraza A, Puerta E, Pérez-Roldán JM, García-Barroso C, Franco R, Aguirre N, García-Osta A (2011) Sildenafil restores cognitive function without affecting β -amyloid burden in a mouse model of Alzheimer's disease. *Br J Pharmacol* 164:2029–2041.
- De Jong LW, Van Der Hiele K, Veer IM, Houwing JJ, Westendorp RGJ, Bollen ELEM, De Bruin PW, Middelkoop HAM, Van Buchem MA, Van Der Grond J (2008) Strongly reduced volumes of putamen and thalamus in Alzheimer's disease: an MRI study. *Brain* 131:3277–3285.
- Drachman DA, Leavitt J (1974) Human memory and the cholinergic system. A relationship to aging? *Arch Neurol* 30:113–121.
- Friston KJ, Bastos AM, Pinotsis D, Litvak V (2015) LFP and oscillations—what do they tell us? *Curr Opin Neurobiol* 31:1–6.
- Gerstein GL, Mandelbrot B (1964) Random walk models for the spike activity of a single neuron. *Biophys J* 4:41–68.
- Giocomo LM, Hussaini SA, Zheng F, Kandel ER, Moser MB, Moser EI (2011) Grid cells use HCN1 channels for spatial scaling. *Cell* 147:1159–1170.
- Haegens S, Náchér V, Luna R, Romo R, Jensen O (2011) alpha-Oscillations in the monkey sensorimotor network influence discrimination performance by rhythmical inhibition of neuronal spiking. *Proc Natl Acad Sci USA* 108:19377–19382.
- Halgren E, Boujon C, Clarke J, Wang C, Chauvel P (2002) Rapid distributed fronto- parieto-occipital processing stages during working memory in humans. *Cereb Cortex* 12:710–728.
- Herrmann S, Stieber J, Ludwig A (2007) Pathophysiology of HCN channels. *Pflügers Arch* 454:517–522.
- Honnuriah S, Narayanan R (2013) A calcium-dependent plasticity rule for HCN channels maintains activity homeostasis and stable synaptic learning. *PLoS One* 8:e55590.
- Hughes SW, Crunelli V (2005) Thalamic mechanisms of EEG alpha rhythms and their pathological implications. *Neuroscientist* 11:357–372.
- Hughes SW, Lorincz ML, Blethyn K, Kékesi KA, Juhász G, Turmaine M, Parnavelas JG, Crunelli V (2011) Thalamic gap junctions control local neuronal synchrony and influence macroscopic oscillation amplitude during EEG alpha rhythms. *Front Psychol* 2:1–11.
- Klimesch W (2012) Alpha-band oscillations, attention, and controlled access to stored information. *Trends Cogn Sci* 16:606–617.
- Krishnan GP, Chauvette S, Shamie I, Soltani S, Timofeev I, Cash SS, Halgren E, Bazhenov M (2016) Cellular and neurochemical basis of sleep stages in the thalamocortical network. *Elife* 5:1–29.
- Kumar A, Singh A, Ekavali (2015) A review on Alzheimer's disease pathophysiology and its management: an update. *Pharmacol Rep* 67:195–203.
- Lánková V, Lánský P, Smith CE (1994) Synaptic transmission in a diffusion model for neural activity. *J Theor Biol* 166:393–406.
- Lőrincz ML, Crunelli V, Hughes SW (2008) Cellular dynamics of cholinergically induced alpha (8–13 Hz) rhythms in sensory thalamic nuclei in vitro. *J Neurosci* 28:660–671.
- Lőrincz ML, Kékesi KA, Juhász G, Crunelli V, Hughes SW (2009) Temporal framing of thalamic relay-mode firing by phasic inhibition during the alpha rhythm. *Neuron* 63:683–696.
- MacManus A, Ramsden M, Murray M, Henderson Z, Pearson HA, Campbell VA (2000) Enhancement of (45)Ca(2+) influx and voltage-dependent Ca(2+) channel activity by beta-amyloid-(1–40) in rat cortical synaptosomes and cultured cortical neurons. Modulation by the proinflammatory cytokine interleukin-1beta. *J Biol Chem* 275:4713–4718.
- McCormick DA, Prince DA (1986) Acetylcholine induces burst firing in thalamic reticular neurones by activating a potassium conductance. *Nature* 319:402–405.
- Narayanan R, Johnston D (2008) The ascent of channels with memory. *Neuron* 60:735–738.
- Rihs TA, Michel CM, Thut G (2007) Mechanisms of selective inhibition in visual spatial attention are indexed by alpha-band EEG synchronization. *Eur J Neurosci* 25:603–610.
- Saito Y, Inoue T, Zhu G, Kimura N, Okada M, Nishimura M, Kimura N, Murayama S, Kaneko S, Shigemoto R, Imoto K, Suzuki T (2012) Hyperpolarization-activated cyclic nucleotide gated channels: a potential molecular link between epileptic seizures and A β generation in Alzheimer's disease. *Mol Neurodegener* 7:50.

- Schreckenberger M, Lange-Asschenfeldt C, Lochmann M, Mann K, Siessmeier T, Buchholz H-G, Bartenstein P, Gründer G (2004) The thalamus as the generator and modulator of EEG alpha rhythm: a combined PET/EEG study with lorazepam challenge in humans. *Neuroimage* 22:637–644.
- Selkoe DJ (1997) Alzheimer's disease—genotypes, phenotype, and treatments. *Science* 275:630–631.
- Tiihonen J, Hari R, Kajola M, Karhu J, Ahlfors S, Tissari S (1991) Magnetoencephalographic 10-Hz rhythm from the human auditory cortex. *Neurosci Lett* 129:303–305.
- Vijayan S, Kopell NJ (2012) Thalamic model of awake alpha oscillations and implications for stimulus processing. *Proc Natl Acad Sci USA* 109:18553–18558.
- Vitiello G (2015) The use of many-body physics and thermodynamics to describe the dynamics of rhythmic generators in sensory cortices engaged in memory and learning. *Curr Opin Neurobiol* 31:7–12.
- Vitiello MV (1989) Dominant occipital (alpha) rhythm frequency in early stage Alzheimer's disease and depression. *Science* 98195:427–432.
- Wu Z, Guo Z, Gearing M, Chen G (2014) Tonic inhibition in dentate gyrus impairs long-term potentiation and memory in an Alzheimer's disease model. *Nat Commun* 5:1–12.
- Destexhe A, Sejnowski TJ (1997) Synchronized oscillations in thalamic networks: insights from modeling studies. *Thalamus* 2:331–371.